



# Electronic transport and optical properties of nano-structured Pt-doped CdO films: evaluate the effect of treatment in hydrogen gas

A. A. Dakhel<sup>1</sup>

Received: 20 September 2017 / Accepted: 17 November 2017 / Published online: 20 November 2017  
© Springer Science+Business Media, LLC, part of Springer Nature 2017

## Abstract

Cadmium oxide (CdO) has various applications related to its natural optoelectronic properties as an oxide, which belongs to group of transparent conducting oxides. However, those properties could be controlled to a desired choice by doping method. For developing the application in the field of optoelectronics, the conduction parameters (conductivity, carrier mobility, and carrier concentration) together with the transparency in the NIR should be improved. Therefore, it is important to seek ways to realise those improvements. Doping method is the way that used to attain that aim. In the present work, CdO thin films doped with different amounts of platinum (Pt) ions were deposited on glass and silicon substrates by the method of physical vapour deposition. The deposited films were characterized by X-ray fluorescence, X-ray diffraction, optical absorption spectroscopy, and electrical measurements. A variety of results was obtained in the present work; the optimum improvement in the electrical properties was found with CdO film doped with 0.13 wt% Pt. A combination of low resistivity ( $1.74 \times 10^{-4} \Omega \text{ cm}$ ), high carrier concentration ( $1.02 \times 10^{21} \text{ cm}^{-3}$ ) and relatively high mobility ( $35.4 \text{ cm}^2/\text{V s}$ ) were obtained under hydrogenation.

## 1 Introduction

Transparent conducting oxides (TCO) have a unique combination of high optical transparency in visible and NIR spectral region and high electrical conductivity. Consequently, they have a wide range of applications, especially in the field of optoelectronic devices. Recently, they received a considerable attention to develop their properties for the highest performance. Metallic oxides like,  $\text{In}_2\text{O}_3$ ,  $\text{Ga}_2\text{O}_3$ ,  $\text{SnO}_2$ ,  $\text{ZnO}$ , and  $\text{CdO}$  are the well known binary compounds of TCO materials. The basic optoelectronic properties of any TCO are generated by natural, non-stoichiometry of oxygen vacancies ( $V_{\text{O}}$ ) and metal interstitials ( $M_i$ ).

CdO has the rock-salt cubic structure of space group (SG) Fm-3m of a lattice parameter of 0.4695 nm [1]. It has a n-type degenerate semiconductor properties with relatively low resistivity ( $10^{-2}$ – $10^{-4} \Omega \text{ cm}$ ), excellent transparency in the NIR spectral region, and translucency in the Vis spectral region. The bandgap of CdO thin films was measured to be in the range ~2.2–2.7 eV depending on the preparation types and conditions [2, 3]. Therefore, CdO has numerous

applications in the solar-cell field and manufacturing of smart windows [2–4].

The optoelectronic properties of CdO could be controlled and developed by doping with different types of impurity ions [5–10]. The present work studied the doping of CdO by  $\text{Pt}^{2+}$  ions since they are smaller than  $\text{Cd}^{2+}$  ions so that they could substitute for  $\text{Cd}^{2+}$  ions in CdO lattice forming substitutional solid solution (SSS) without introducing a great distortion to the CdO lattice unit cell (UC). In addition, Pt is a good conductor and considered as a good catalyst in dissociation of  $\text{H}_2$  molecules, which was used in the present work as an annealing atmosphere [11]. Therefore, doping of CdO with platinum ions is expected to improve its electronic transport properties. It is to be mentioned that a study of optoelectronic properties of Pt-doped CdO was not conducted yet elsewhere, although it was carried out for other TCO's like ZnO [12, 13],  $\text{SnO}_2$  [14], and  $\text{In}_2\text{O}_3$  [15]. However, the optical properties of sol-gel Pt-doped CdO were studied in Ref. [16]. As many investigations on doping of host CdO with different types of ions were carried out in order to improve its TCO properties, thus, the results of the present work have to be compared with those results obtained previously for similar ions doping.

✉ A. A. Dakhel  
adakhil@uob.edu.bh

<sup>1</sup> Department of Physics, College of Science, University of Bahrain, P.O. Box 32038, Manama, Kingdom of Bahrain

## 2 Experimental details

Cadmium oxide (CdO) incorporated with different amounts of platinum (Pt) ions thin films were deposited on glass and Si substrates. A fine powder of platinum-oxide hydrate ( $\text{PtO}_2 \cdot \text{H}_2\text{O}$ ) of analytical grade (from Sigma-Aldrich) was utilised as a source of dopant Pt ions. The starting materials, pure fine CdO and  $\text{PtO}_2 \cdot \text{H}_2\text{O}$  powders, were alternatively (layer-by-layer) evaporated in a residual oxygen atmosphere of  $\sim 1.3 \times 10^{-3}$  Pa by using ceramic baskets (Midwest tungsten service). The used Corning 2947 glass substrates (from Sigma-Aldrich) were ultrasonically cleaned in distilled water, acetone, alcohol and then dried while the silicon wafers were cleaned with acetone, deionized water, and KOH solution. The Si-wafer substrates were used sol for XRF measurements. The evaporated masses were controlled with the help of a piezoelectric microbalance crystal sensor (type Philips FTM5) fixed close to the substrates. Then, the as-grown films were flash annealed in the air at the 400 °C for 1 h keeping samples inside the closed furnace for a slow cool to the room temperature. The thickness of each film was measured after annealing by a MP100-M spectrometer (Mission Peak Optics Inc., USA), to be in the range 0.10–0.20  $\mu\text{m}$ . The Pt to Cd weight ratio content of each sample was estimated by X-ray fluorescence (XRF) method with an Amptek XR-100CR (USA) XR detector of energy resolution 180 eV controlled by a built-in MCDWIN 3.1 program. The measured Pt/Cd mass ratios were  $\sim 0.07$ ,  $\sim 0.13$ , and  $\sim 0.20\%$  for the sample S1, S2, and S3, respectively.

The crystal structure of the samples was investigated and analyzed by a Rigaku Ultima-VI X-ray diffractometer using  $\text{Cu } K_\alpha$  rays. The Rietveld structural analyses were carried out by a built-in PDXL program. The spectral optical transmittance,  $T(\lambda)$  and normal reflectance,  $R(\lambda)$  were measured in a spectral range of 300–2000 nm with a Shimadzu UV-3600 double beam spectrophotometer. The double-beam regime of the spectrophotometer was used to exclude the effect of small absorption by the substrates (for  $\lambda > 245$  nm). The dc-electrical measurements of conductivity ( $\sigma$ ), carrier mobility ( $\mu_{el}$ ), and carrier concentration ( $N_{el}$ ) were conducted by a standard Van der Pauw method of  $\sim 1$  T magnetic field.

## 3 Structure analysis

The element's content of each film grown on silicon substrate was determined by the X-ray fluorescent (XRF) method. Figure 1 shows the XRF spectrum of one sample. The spectrum demonstrates Cd L-band (3.13–3.53 keV)

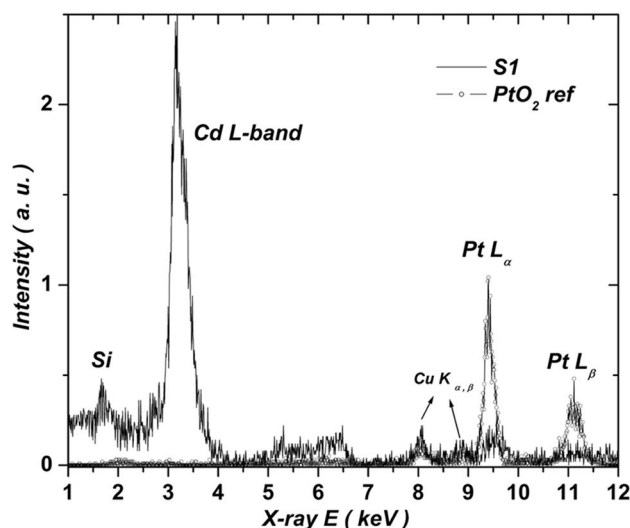
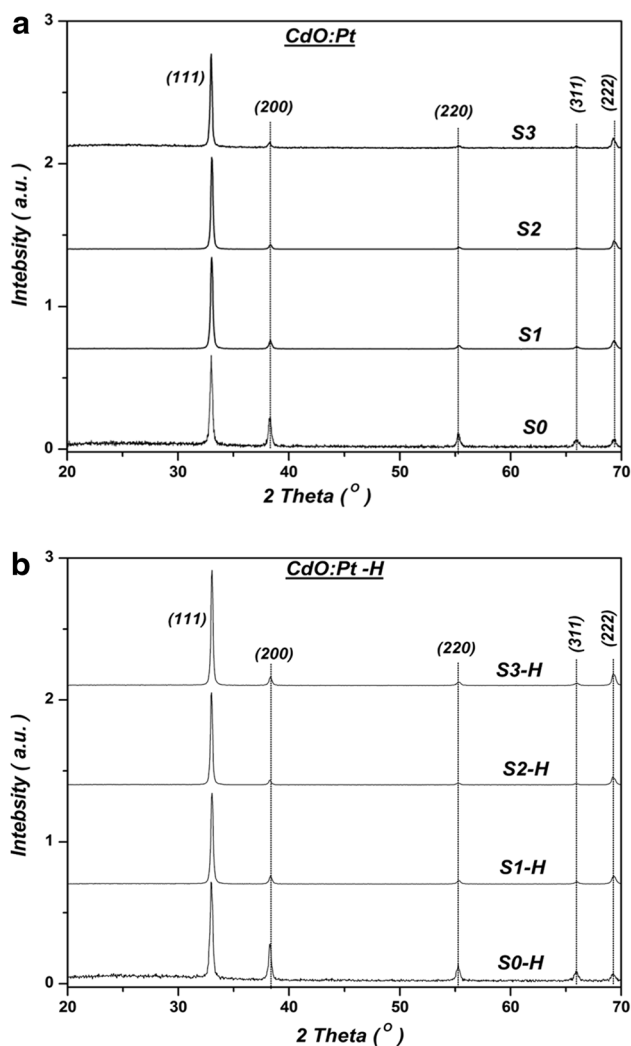


Fig. 1 XRF spectrum of sample S1 (multiply by 2) and reference  $\text{PtO}_2$  films on Si wafers

and Pt L-signals (9.44 and 11.07 keV) with the Si substrate  $K\alpha$ -signal (1.74 keV) and source Cu K-signals (8.04 and 8.9 keV). This spectrum confirms the purity of the prepared sample. The ratio of the integrated intensity of Pt- $L_\alpha$  band to that of the Cd L-band was used to determine the fractional weight ratio Pt/Cd in each film sample. For that purpose, a known method of micro radiographic analysis was utilized [17]. The reference samples were  $\text{PtO}_2$  and CdO thin films grown on Si substrates. The measured Pt/Cd mass ratios were 0.07, 0.13, and 0.20% for the sample S1, S2, and S3, respectively.

The XRD patterns of undoped and Pt-doped CdO films deposited on glass substrates are shown in Fig. 2a. The X-ray peaks were indexed according to the known standard cubic structure (Fm-3m) [1]. The XRD patterns reveal that the energetically preferred [111] orientation of undoped CdO films was enhanced by Pt-ions doping. The variation in the level of preferred orientation growth of the investigated films due to the incorporation of Pt ions confirmed the realization of the doping process of Pt ions in the host lattice of CdO. The growth degree of preferential orientation in [111] direction can be studied through a texture coefficient (TC) [18];  $\text{TC}_{[111]} = [n_{[111]}/I_{0[111]}]/[\sum I(h'k'l')/I_0(h'k'l')]$ , where  $I_{[hkl]}$  and  $I_{0[hkl]}$  are the integrated intensities of certain [hkl] reflection from the film sample and the standard polycrystalline powder, which quoted from ref [1]. The sum in the equation runs over the total number ( $n=4$ ) of the recorded reflections shown in Fig. 2. The values of  $\text{TC}_{[111]}$  (Table 1) show that Pt doping increased  $\text{TC}_{[111]}$  up to the highest value of 3.3 (out of 4) for S2, then slightly reduced to 3.2 for S3. The enhancement of [111] orientation of the host CdO film was also observed in the case of other metallic dopants like Fe, Cr, Ce [6, 19, 20]. As  $\text{TC}_{[111]}$  is considered as a level of



**Fig. 2** **a** XRD patterns of pristine and Pt-doped CdO films. **b** XRD patterns of hydrogenated pristine and Pt-doped CdO films

crystallinity, then its variation with doping level should be related to the variation of carrier mobility and mean-free-path (mfp) (next paragraph—Fig. 5a).

Figure 2a reveals that doping by Pt ions did not modify the ordinary cubic crystalline structure of host CdO. Furthermore, the XRD patterns of Pt-doped CdO samples show the absence of peaks arising from pure, oxide or any Pt related phases, which confirms the total doping of Pt ions into the CdO lattice, without formation of separate Pt phases within CdO lattice.

The structural analyses of Fig. 2 are presented in Table 1. The lattice parameter ( $a$ ) was calculated by a Rietveld refinement method using acceptable values of R-parameters ( $R_{wp}$  is the weighted profile factor and  $\chi^2$  is the goodness-of-fit) for good fitting [21]. The bulk volume strain ( $\epsilon_{vs}$ ) measures the change of UC volume:  $\epsilon_{vs} = \Delta v_{UC}/v_{UC}^0 = (v_{UC}/v_{UC}^0) - 1$ , where  $v_{UC}^0$  is the UC volume of the reference undoped CdO film. The data on Table 1 indicate shrinking in host UC with doping (i.e.  $\epsilon_{vs} < 0$ ) due to the smaller ionic radius of dopant  $Pt^{2+}$ , 0.80 versus 0.95 Å for  $Cd^{2+}$  [22]. The difference between radii of  $Pt^{2+}$  and  $Cd^{2+}$  ions (~15%) follows Hume-Rothery rule [23] about the possibility of formation of substitutional solid solution (SSS). Therefore, the volume of UC ( $v_{UC}$ ) of host CdO changed with the doping level. It attained the lowest value of S2 sample, and then increased to that value of sample S3. It can be concluded that part of the additional Pt ions of S3 was accumulation on its grain- and crystallite-boundaries (GB and CB) rather than really doped into the CdO lattice.

The average crystallite size (CS) with the structural strain ( $\epsilon_{ss}$ ) was calculated for each sample by using graphical Williamson–Hall method, as shown in Fig. 3 for sample S2. The nano-CS given in Table 2, increased with doping level to the largest value for S2. The decreasing of CS for S3 might be explained by the accumulation of dopant ions on GB/CB due to the solid solubility limit (saturation) of Pt ions in CdO lattice.

**Table 1** The structural parameters of the studies pure and Pt-doped CdO films; lattice parameter ( $a$ ),  $\epsilon_{vs}$  is the UC volume (bulk) strain, Rietveld refinement parameters ( $R_{wp}$ ) and ( $\chi^2$ ), average crystallites size (CS), structural micro strain ( $\epsilon_{ss}$ ), and [111]-texture coefficient ( $TC_{(111)}$ )

Sample	$a$ (Å)	$\epsilon_{vs} (\times 10^{-3})$	$R_{wp}$ (%)	$\chi^2$ (%)	CS (nm)	$\epsilon_{ss}$ (%)	$TC_{(111)}$
S0	4.7016	Ref.	25.7	1.5334	30.4	0.15	1.8
S1	4.6919	−6.2	13.02	1.8973	34.5	0.18	2.9
S2	4.6889	−8.1	13.25	2.9983	41.9	0.18	3.3
S3	4.6943	−4.6	11.92	1.2354	28.1	0.19	3.2
Hydrogenated samples		$\epsilon_{vs}^H (\times 10^{-3})$					
S0-H	4.6987	−1.8	19.78	1.9174	29.6	0.14	2.50
S1-H	4.6945	+1.7	12.31	1.9676	30.6	0.16	2.97
S2-H	4.6923	+2.2	12.27	2.6316	35.9	0.16	3.30
S3-H	4.6940	~0	13.95	2.0846	32.7	0.15	2.92

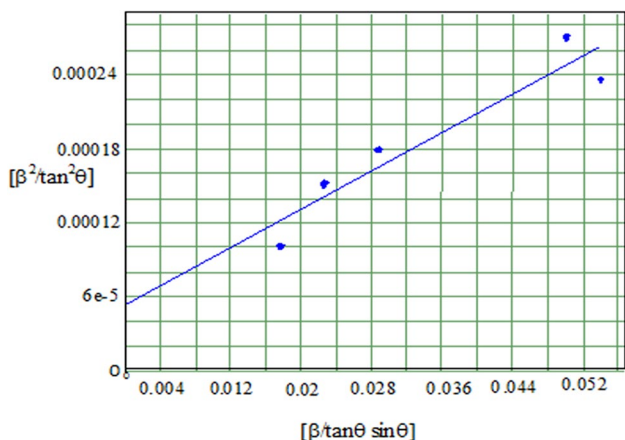


Fig. 3 Williamson–Hall for S2 film sample

Figure 2b presents the XRD patterns of hydrogenated samples. Hence, the hydrogenation did not introduce any change in the SG of CdO films. However, a small change in the lattice parameter was introduced to the host CdO, as presented in Table 1. To study the effect of hydrogenation on the UC volume of each sample, the following volume strain was defined as:

$$\epsilon_{vs}^H = \Delta v_{HUC}/v_{UC} = (v_{HUC}/v_{UC}) - 1,$$

where  $v_{HUC}$  is the UC volume of any hydrogenated sample and  $v_{UC}$  is the volume of the corresponding non-hydrogenated sample. Thus, the volume of host UC was increased for doped CdO samples, S1–H and S2–H due to the creation of O-vacancies, since Pt ions is an active catalyst to dissociate H<sub>2</sub> molecules into H ions/atoms [11], which interact with the structural oxygen ions removing them to produce O-vacancies. For S3–H the adsorbed H<sub>2</sub> molecules were dissociated by the Pt ions those accumulated on GBs and CBs, therefore the volume of UC inside the crystallites did not (or slightly) change. Notice that for undoped CdO–H, the

H<sub>2</sub> molecules did not dissociate and thus the variation in UC volume is due to the usual annealing effects.

### 4 Electrical properties

The measured conduction parameters (CPs):  $\sigma$ ,  $\mu_{el}$ , and  $N_{el}$  of undoped and Pt-doped CdO films are presented in Fig. 4 and Table 2. Therefore, the CPs of the host CdO films were developed by increasing Pt% incorporation level to 0.13 wt% with sample S2, after which they gradually deteriorated for sample S3. That deterioration in sample S3 could be explained by the accumulation of part of the additional Pt ions over the content of S2 on CBs and GBs. Such accumulation creates a potential barrier that effectively reduces the concentration of carriers and conductivity. Thus, the electrical results are in agreement with the structural results, especially the TC[111] and CS (Table 1), which reach their largest values of S2 sample before deterioration with S3 sample. Figure 5 shows a similar behavior of TC<sub>[111]</sub> and carrier mobility ( $\mu_{el}$ ) versus doping level. Moreover, the conduction could be studied through a carrier mean-free-path ( $mfp$ ), which defined as  $mfp = (h/2e)(3N_{el}/\pi)^{1/3} \mu_{el}$ , where  $h$  is the Planck constant and  $e$  is the electronic charge [24]. The variation in the  $mfp$  among the samples was plotted in Fig. 5. It is clear that the trends of  $mfp$  and  $\mu_{el}$  versus doping level are identical, which means that the  $mfp$  is mainly controlled by carrier scattering elements. This also means that there is some relationship between the  $mfp$  and density of structural defect density (or crystallinity);  $D = (CS)^{-2}$ , which can be observed in the inset of Fig. 5a. The main difference between Fig. 5a, b is the reduction of the  $\mu_{el}$  at higher doping level of Fig. 5b for hydrogenated sample, which refer to increasing of carrier scattering by the accumulated H atoms/ions at GBs/CBs and in host CdO lattice.

Finally, it is to be mentioned here that by comparing with those electrical results obtained by previous investigations

**Table 2** The measured electrical conduction parameters ( $\rho$ ,  $\mu_{el}$ , and  $N_{el}$ ), electronic mean free path ( $mfp$ ), optical absorption coefficient at 1000 nm, and optical band gap ( $E_g$ ), for undoped and Pt-doped CdO films

Sample	$\rho$ ( $\times 10^{-4}$ $\Omega$ cm)	$\mu_{el}$ ( $cm^2/V$ s)	$N_{el}$ ( $\times 10^{20}$ $cm^{-3}$ )	$mfp$ (nm)	$\alpha(1000$ nm) ( $\times 10^4$ $cm^{-1}$ )	$E_g$ (eV)
S0	201	7.03	0.44	0.51	0.3540	2.25
S1	5.92	34.92	3.02	4.78	4.35	2.06
S2	3.6	41.63	4.17	6.34	5.02	2.15
S3	8.15	41.48	1.85	4.60	3.75	2.11
Hydrogenated samples						
S0-H	69.1	8.5	1.05	0.81	0.5153	2.28
S1-H	2.41	28.54	9.08	5.63	4.858	2.09
S2-H	1.74	35.42	10.13	7.25	5.04	2.26
S3-H	3.69	30.60	5.53	4.90	2.916	2.25

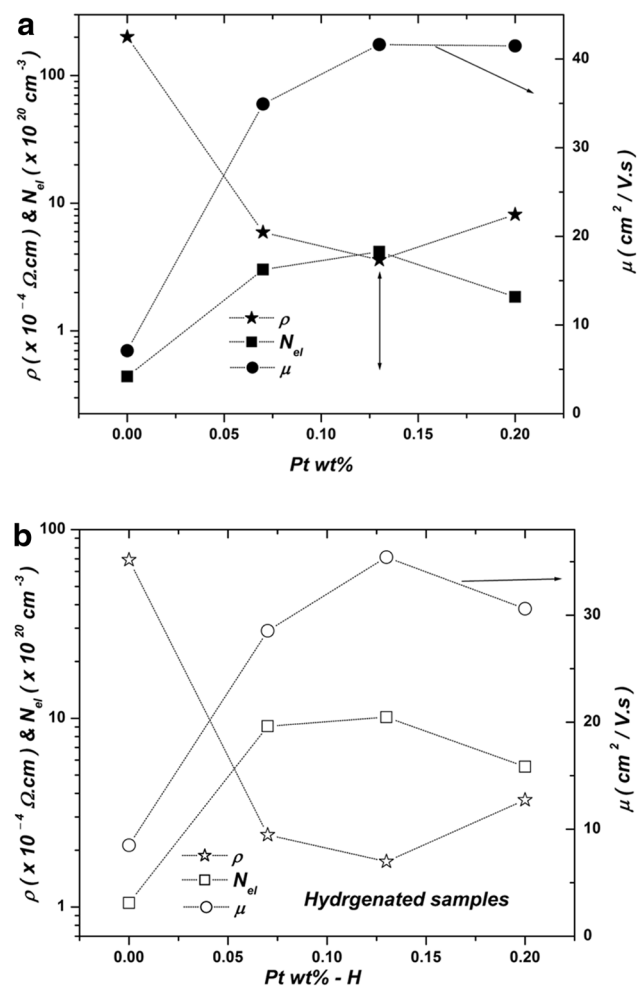


**Fig. 4** **a** Conduction parameters variations with Pt doping level in the film samples. **b** Conduction parameters variations with Pt doping level in the hydrogenated film samples

conducted on host CdO films doped with different ions, the present electrical results are comparable to those obtained with W-doped CdO films [9]. However, the present electrical results are not superior as those in case of CdO doped with Al or Ge [25, 26] ions.

## 5 Optical properties

The wavelength dependence of corrected transmittance,  $T(\lambda)$  of undoped and Pt-doped CdO films are presented in Fig. 6a. It is clear that, the studied films are translucent in the visible region tending to be almost transparent in the NIR spectral region.

The spectral reflectance,  $R(\lambda)$  of the studied films/glass substrates is shown in Fig. 4a revealing that  $R$  is small and almost constant of  $<5\%$ . The spectral absorbance  $A(\lambda)$  of the present films was calculated by  $A(\lambda) = \ln[(1 - R(\lambda))/T(\lambda)]$ .

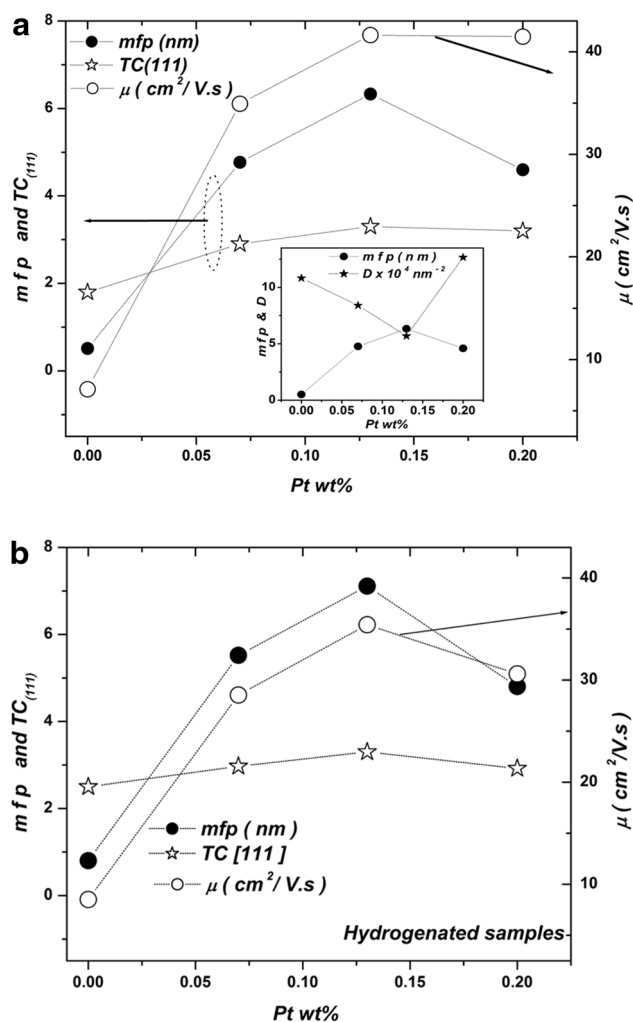


**Fig. 5** **a** Variation of mfp,  $TC_{[111]}$ , and  $\mu$  with Pt doping level in the film samples. The inset shows the variation of mfp and structural defect density (D) with Pt doping level in the film samples. **b** Variation of mfp,  $TC_{[111]}$ , and  $\mu$  with Pt doping level in the hydrogenated film samples

The spectral absorption (attenuation) coefficient  $\alpha(\lambda)$  is related to the absorbance  $A(\lambda)$  by  $A(\lambda) = \alpha(\lambda) \times d$ , where  $d$  is the thickness of the film. Therefore, the optical band gap ( $E_g$ ) can be evaluated for each film by the well-known Tauc technique [27, 28]:

$$\alpha h\nu = A_{op}(h\nu - E_g)^m \quad (1)$$

where  $h\nu$  is the photon energy,  $m$  is equal to 0.5 for direct transitions and  $A_{op}$  is the constant of each film sample. Figure 7a shows  $(A \cdot h\nu)^2$  versus  $h\nu$  plot; the extrapolation of the straight-line portion to  $(A \cdot h\nu)^2 = 0$ —line gives the value of the band gap (Table 2) with an estimated accuracy within 0.05 eV. The bandgap of undoped CdO was obtained to be within the known standard range of values [4]. With Pt



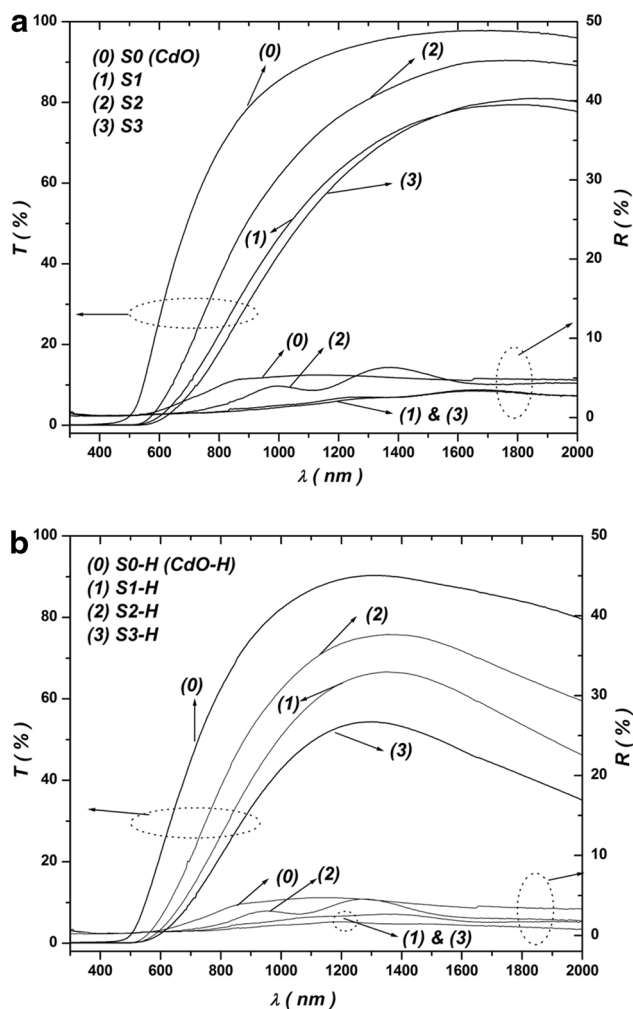


**Fig. 6** **a** Transmittance,  $T(\lambda)$  and reflectance,  $R(\lambda)$  spectra of pristine and Pt-doped CdO films. **b** Transmittance,  $T(\lambda)$  and reflectance,  $R(\lambda)$  spectra of hydrogenated pristine and Pt-doped CdO films

doping, the bandgap of host CdO films were red-shifted by different values. However, that bandgap narrowing (BGN) of host CdO, due to Pt-doping, was found to go together with increasing in carrier concentration (Table 2). Such observation is clearly in contrast with the known Moss–Burstein (B–M) effect [29]. Therefore, it should be proposed that doping of host CdO with Pt ions induces two contrary phenomena, i.e. the bandgap narrowing (BGN) in addition to the bandgap widening BGW. The BGN is attributed to the change in the electron–lattice interactions due to the insertion of dopant impurity ions generating impurity band tail broadening that emerges with the conduction band causing BGN [30, 31]. The BGN was also observed in Pt-doped CdO samples prepared by the sol gel method [16].

The optical properties of the present samples were changed by hydrogenation, as shown in Fig. 6b. Generally the effect of hydrogenation is to create more O-vacancies

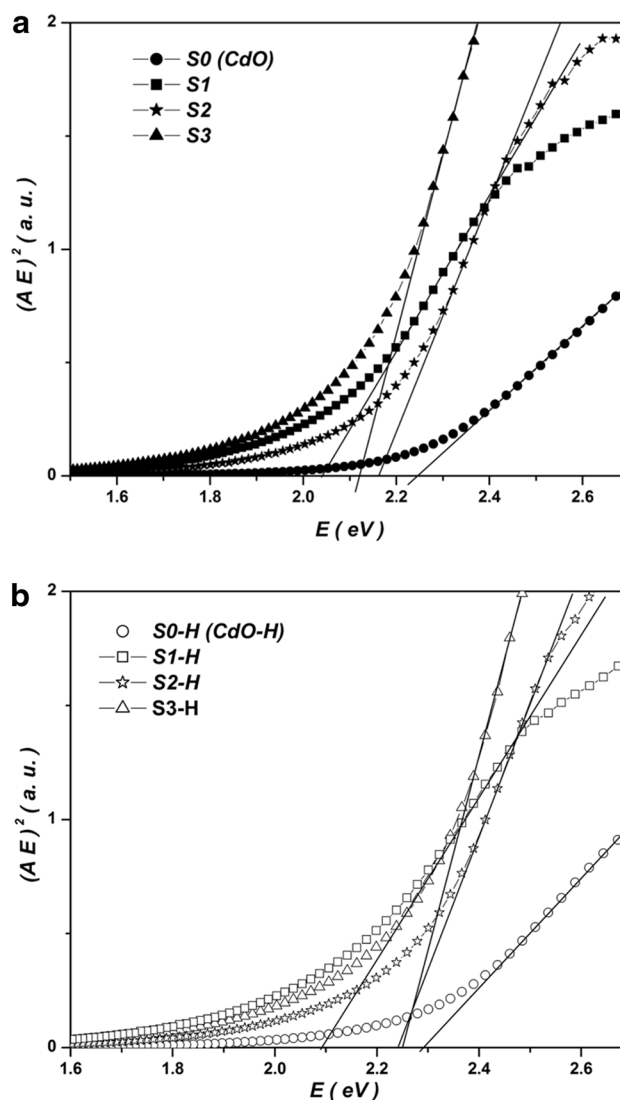


**Fig. 7** **a** Tauc plot for pristine and Pt-doped CdO films. **b** Tauc plot for hydrogenated pristine and Pt-doped CdO films

together with more carrier concentration. The observed hydrogenation effect could be studied by comparing Fig. 6a with Fig. 6b that show clear damping at high-wavelength side of the  $T(\lambda)$  spectra, which caused by increasing the density of carriers created by the hydrogenation. The lowest damping rate is that with undoped CdO sample, which refers to the lowest created density of O-vacancies and carriers.

In summary, the presence of dopant  $Pt^{2+}$  dopant ions in host CdO has the efficient ability for dissociate  $H_2$  molecules into H atoms/ions that could create more O-vacancies, thus, increase the density of conduction electrons, which increases the absorption at high-wavelength NIR side of the  $T(\lambda)$  spectra. The change of optical bandgap due to the hydrogenation was studied, as shown in Fig. 7b and Table 2. It is clear that the hydrogenation increases the bandgap in different values

depending on the carrier concentration, according to B–M effect.

It was observed that the optical absorption coefficient ( $\alpha$ ) in the translucent spectral region of host CdO films depends on the Pt<sup>2+</sup>doping level. At 1000 nm (NIR) data on the absorption coefficient [ $\alpha(1000\text{ nm})$ ] are presented in Table 2. Figure 8 demonstrates the variation of  $\alpha(1000\text{ nm})$  with  $N_{el}$  for the studied samples before and after hydrogenation. In both cases,  $\alpha(1000\text{ nm})$  increased with increasing of  $N_{el}$ , which was expected. However, values of  $\alpha(1000\text{ nm})$  decreased with hydrogenation, although  $N_{el}$  increased. That can be explained by the structural changes induced during the hydrogenation. The hydrogenation introduced a variation in dopant ion distribution by tossing the incorporated dopant ions for more homogenization, created O-vacancies, and accumulated some H atoms/ions inside the host CdO film, in addition to the enhancement of carrier concentration  $N_{el}$ . These Opto-absorbing factors are negligible for undoped CdO, as shown in Fig. 8.

## 6 Conclusions

CdO thin films incorporated with different amount of Pt ions were prepared by evaporation method. Such doping was expected to improve the TCO properties of CdO films, especially after hydrogenation since Pt ions could assist to dissociate H<sub>2</sub> molecules into H ions. The structural study of the prepared Pt-doped CdO showed that it is possible to prepare CdO films totally doped with Pt<sup>2+</sup> ions with concentration up to ~0.13 wt%. It was found Pt doping to have a strong effects

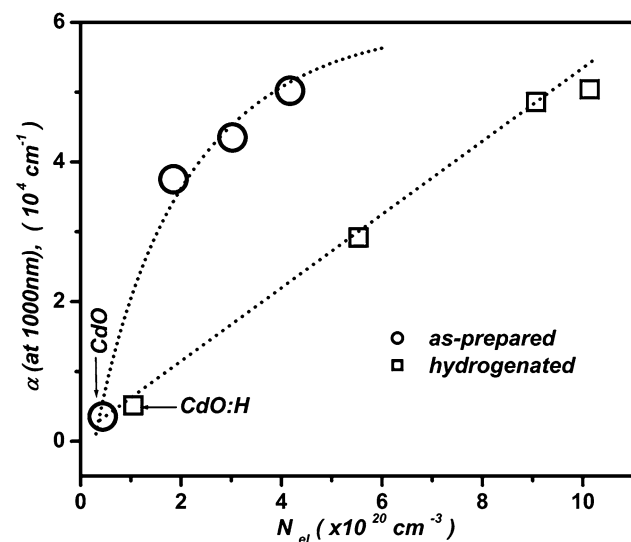


**Fig. 8** Variation of absorption coefficient  $\alpha$  at 1000 nm with electronic concentration for the as-prepared and hydrogenated pristine and Pt-doped CdO films

on the structural, optical and electrical properties of host CdO films. It was found the Pt doping strongly enhanced the [111] preferred orientation growth of CdO films up to ~83% of complete [111] orientation. Moreover, Pt doping caused a red shift to the optical bandgap of the host CdO. The hydrogenation of the Pt-doped films was found to improve the conduction TCO parameters, especially the conductivity and mobility, which was the aim of the present work. The utmost conduction combination enhancement of mobility (35.4 cm<sup>2</sup>/V s), conductivity (5.74 × 10<sup>3</sup> S/cm) and carrier concentration (1.02 × 10<sup>21</sup> cm<sup>-3</sup>) was found with CdO films doped with ~0.13 wt% Pt. These results confirm the possibility of to utilise pt-doped CdO films in TCO applications.

## References

1. Powder Diffraction File, Joint Committee for Powder Diffraction Studies (JCPDS) file No. 05-0640
2. B.G. Lewis, D.C. Paine, Mater. Res. Soc. Bull. **25**, 22 (2000)
3. M. Yan, M. Lane, C.R. Kannewarf, R.P.H. Changa, Appl. Phys. Lett. **78**, 2342 (2001)
4. Z. Zhao, D.L. Morel, C.S. Ferekides, Thin Solid Films **413**, 203 (2002)
5. P.K. Gupta, K. Ghosh, R. Patel, S.R. Mishra, P.K. Kahol, Curr. Appl. Phys. **9**, 673 (2009)
6. A.A. Dakhel, Thin Solid Films **518**, 1712 (2010)
7. A.A. Dakhel, J. Alloys Compd. **475**, 51 (2009)
8. A.A. Dakhel, Adv. OptoElectron. **2013**, 804646 (2013)
9. A.A. Dakhel, J. Electron. Mater. **41**, 2405 (2012)
10. R.K. Gupta, F. Yakuphanoglu, F.M. Amanullah, Physica E **43**, 1666 (2011)
11. Y. Park, G. Kim, Y.H. Lee, Appl. Phys. Lett. **92**, 083108 (2008)
12. N. Tamaekong, C. Liewhiran, A. Wisitsoraat, S. Phanichphant, Sensors **9**, 6652 (2009)
13. A. Hastir, N. Kohli, R.C. Singh, Proceedings of the World Congress on Recent Advances in Nanotechnology (RAN'16) Prague, Czech Republic—April 1–2, 2016 Paper No. ICNEI 105. <https://doi.org/10.11159/icnei16.105>
14. Y. Shen, T. Yamazaki, Z. Liu, D. Meng, T. Kikuta, J. Alloys Compd. **488**, L21 (2009)
15. D. Selvakumar, P. Rajeshkumar, N. Dharmaraj, N.S. Kumar, Mater. Today **3**, 1725 (2016)
16. Z. Serbetci, B. Gunduz, A.A. Al-Ghamdi, F. Al-Hazmic, K. Arik, F. El-Tantawy, F. Yakuphanoglu, W.A. Farooq, Acta Phys. Pol. A **126**, 798 (2014)
17. J.M. Jaklevic, F.S. Goulding, in *Energy Dispersion in X-ray Spectrometry*, ed. by H.K. Herglotz, L.S. Birks (M. Dekker, New York, 1978)
18. C.S. Barrett, T.B. Massalski, *Structure of Metals* (Pergamon, Oxford, 1980)
19. A.A. Dakhel, H. Hamad, Int. J. Thin Films Sci. Technol. **1**, 25 (2012)
20. A.A. Dakhel, Mater. Chem. Phys. **130**, 398 (2011)
21. L.B. McCusker, R.B. Von Dreele, D.E. Cox, D. Louer, P. Scardi, J. Appl. Cryst. **32**, 36 (1999)
22. R.D. Shannon, Acta Crystallogr. A **32**, 751 (1976)
23. C. Kittel, *Introduction to Solid State Physics* (Wiley, New York, 1996)
24. M. Chen, Z.L. Pei, X. Wang, Y.H. Yu, X.H. Liu, C. Sun, L.S. Wen, J. Phys. D **33**, 2538 (2000)

25. R.K. Gupta, K. Ghosh, R. Patel, S.R. Mishra, P.K. Kahol, *Curr. Appl. Phys.* **9**, 673 (2009)
26. A.A. Dakhel, *Solid State Sci.* **25**, 33 (2013)
27. J. Tauc, F. Abelesn eds., *Optical Properties of Solids* (North Holland, Amsterdam, 1969)
28. M. Mohammadikish, F. Davar, M.R. Loghman-Estarki, Z. Hamidi, *Ceram. Int.* **39**, 3173 (2013)
29. J.I. Pankove, *Optical Processes in Semiconductors* (Dover, New York, 1975)
30. Y.Z. Zhang, J.G. Lu, Z.Z. Ye, H.P. He, L.P. Zhu, B.H. Zhao, L. Wang, *Appl. Surf. Sci.* **254**, 1993 (2008)
31. Y. Dou, R.G. Egdell, T. Walker, D.S.L. Law, G. Beamson, *Surf. Sci.* **398**, 241 (1998)